Chemical Engineering Journal xxx (2018) xxx-xxx

Contents lists available at ScienceDirect

Chemical Engineering Journal

journal homepage: www.elsevier.com

Interaction between bovine serum albumin and mesoporous silica nanoparticles functionalized with biopolymers

Valentina Nairi[a], Sara Medda[a], Marco Piludu[b], Maria Francesca Casula[a], Maria Vallet-Regì[c,*], Maura Monduzzi[a,*], Andrea Salis[a,*]

[a] Dipartimento di Scienze Chimiche e Geologiche, Università di Cagliari-CSGI and CNBS, Cittadella Universitaria, S.S. 554 bivio Sestu, 09042 Monserrato, Cagliari, Italy
[b] Dipartimento di Scienze Biomediche, Università di Cagliari, Cittadella Universitaria, S.S. 554 bivio Sestu, 09042 Monserrato, Cagliari, Italy
[c] Departamento de Quimica Inorganica y Bioinorganica, Facultad de Farmacia, Universidad Complutense de Madrid, Plaza Ramon y Cajal s/n, Instituto de Investigacion Sanitaria Hospital 12 de Octubre i+12 ¡ Centro de Investigacion Biomedica en Red de Bioingenieria, Biomateriales y Nanomedicina (CIBER-BBN), Madrid, Spain

ARTICLE INFO

Keywords:
Mesoporous silica nanoparticles
Hyaluronic acid
Chitosan
Bovine serum albumin
Protein corona
Gold nano particles

ABSTRACT

Biomedical application of nanoparticles is largely associated to their fate in biological media which, in turn, is related to their surface properties. Surface functionalization plays a key role in determining biodegradation, cytotoxicity and biodistribution through interactions which may be mediated by the macromolecules occurring in biological media. A typical example is given by several proteins which lead to the formation of coated nanoparticles referred as protein corona. In this work we focus on mesoporous silica nanoparticles which, due to their intrinsic textural features, show potential as carriers for sustained drug release. Mesoporous silica nanoparticles functionalized by different biopolymers such as hyaluronic acid and chitosan were synthesized and characterized through small angle X-rays scattering, thermal analysis, and infrared spectroscopy. Biopolymer-coated mesoporous silica nanoparticles were used to investigate the interaction with bovine serum albumin, and to point out the role of different biopolymer coating. Gold-conjugated-bovine serum albumin was used to gain evidence on the occurrence of surface bound proteins enabling direct observation by transmission electron microscopy. Our findings provide insights on how different biopolymers affect the formation of a protein corona around functionalized mesoporous silica nanoparticles.

1. Introduction

Cancer is treated with chemotherapeutic drugs which are able to restrain tumor's growth but are also toxic for healthy cells, thus resulting in adverse side effects [1,2]. The use of smart pharmaceutical formulations, which release the drug at the target diseased tissue only, would permit to reduce undesired side effects of the chemotherapeutics [3–6]. In this context, researchers are focusing on nanomaterials as smart carriers for targeted drug delivery and stimuli-responsive systems, useful for the treatment of cancer [7–13].

Ordered mesoporous silicates, synthesized for the first time in the early 1990s [14], are nanostructured materials with a big potential in nanomedicine applications [15–20]. Among them mesoporous silica nanoparticles (MSNs) are likely the best drug carrier candidates for the realization of innovative pharmaceutical formulations [11,21–24], as a result of their characteristic textural and structural features. Indeed, their high surface area (up to 1400 m^2/g), the narrow distribution of pore size (1–2 Å), and the high pore volume (1–3 cm^3/g), allow to load high amounts of drugs which can then be released with a sustained rate [24–26]. Moreover, the external surface of MSNs can easily be functionalized with target biomolecules, i.e. proteins/antibodies [27–29], peptides [30,31] or saccharides [32–34], that can be recognized by receptors overexpressed by tumor cells [35–37]. Alternatively, these macromolecules can modify their conformation, as a response to a change of environmental conditions (i.e. pH), thus acting as a stimuli-responsive system [38,39]. In general, the external functionalization affects MSNs biocompatibility, biodistribution, pharmacokinetics, particle stability, circulation time, tumor accumulation, cellular uptake, and therapeutic efficacy [32,40,41]. Relevant examples of biopolymers for the external functionalization of MSNs surface are offered by hyaluronic acid (HA) and chitosan (CHIT). The first was used by Zhan

* Corresponding authors.
Email address: asalis@unica.it (A. Salis)

https://doi.org/10.1016/j.cej.2018.01.011
Available online xxx
1385-8947/

et al. to obtain a MSNs-based target system. Indeed, tumor cells overexpress CD-44 receptors which recognize HA chains promoting HA-functionalized MSNs' endocytosis, and thus drug internalization in the tumor tissue [1]. CHIT biopolymer, due to its capacity to change conformation depending on pH, was used to realize a pH-responsive system that allows for drug release at the acidic pH of tumor cells [42].

When dispersed in a biological medium, nanoparticles (NPs) seek to lower their surface energy by adsorbing biomolecules such as proteins, peptides, or glycolipids. This surface layer of biomolecules, known as the "protein corona" (PC), is due to the physico-chemical interactions established between the NPs and the biomolecules occurring in the biological fluid [43,44]. The nature of the PC depends on several NPs features [45], such as, their chemical composition [46], size [47], shape [48], surface charge [49–51], and hydrophilic/hydrophobic character [49]. PC also depends on the composition of the biological medium, and on proteins concentration in blood plasma, temperature, administration route as well as composition of the cell membrane [43,51]. Overall, the formation of the PC on NPs surface modifies their physico-chemical properties [11] that is, surface charge and hydrophilic/hydrophobic character, thus affecting the fate of NPs in terms of cellular uptake, [52] and cytotoxicity [53]. Two types of protein corona can occur, the "*hard corona*" (HC), characterized by strong interactions between NPs and proteins, and the "*soft corona*" (SC) consisting of weakly bound proteins [44,52,54]. The formation of either HC or SC depends on medium composition including protein concentration, but also on the NPs external charge, and the affinity of proteins for the NPs surface [51]. Proteins like serum albumins, and immunoglobulins have high concentrations in the blood, therefore they are initially present in the SC of NPs, but they can be replaced, at later time, by other proteins which occur with lower concentrations but show higher affinities toward NPs [55]. These changes of composition in the PC are known as the "Vroman effect" [55,56]. An important factor for the formation of the protein corona is the surface charge of NPs. As demonstrated by Shahabi et al. positive MSNs, functionalized with amine or polyethylene imine, promote the interaction with BSA. On the contrary neutral or negative MSNs, modified with polyethylene glycol or sulfonate, contrast the adsorption of BSA due to the establishment of unfavorable interactions [57]. Recently, we investigated the different behavior of MSNs functionalized with HA or CHIT (MSN-HA and MSN-CHIT respectively) toward cell internalization [32]. In vitro studies showed that the MSN-HA were easily internalized by 3T3 mouse fibroblast cells whereas MSN-CHIT gave rise to large aggregates in the cell medium which prevented an effective cell internalization. A possible reason of this behavior is that the components of the cell medium are adsorbed at a different extent on the functionalized MSNs due to their opposite surface charge. That is negative and positive for MSN-HA and MSN-CHIT respectively. Albumins are negatively charged at pH 7 (IEP ~ 4.7) and are abundant in the cell medium. We hypothesized therefore that albumins would adsorb more effectively on MSN-CHIT than on MSN-HA when forming a PC. This would reduce MSN-CHIT colloidal stability by promoting aggregation [32].

Here the interactions between bovine serum albumin (BSA) with MSN-HA and MSN-CHIT samples are investigated. The aim of the work is to study a model system which may provide new insights on the formation of a PC around MSNs functionalized with oppositely charged biopolymers (HA *vs* CHIT). To this purpose the adsorption of BSA on differently functionalized MSNs (MSN-NH_2, MSN-HA and MSN-CHIT) was investigated through FTIR, zeta potential, and thermogravimetric analysis. Finally, gold nanoparticles conjugated to bovine serum albumin (BSA-GNPs) were used to visualize the bound proteins on MSNs surface by mean of transmission electron microscopy (Scheme 1).

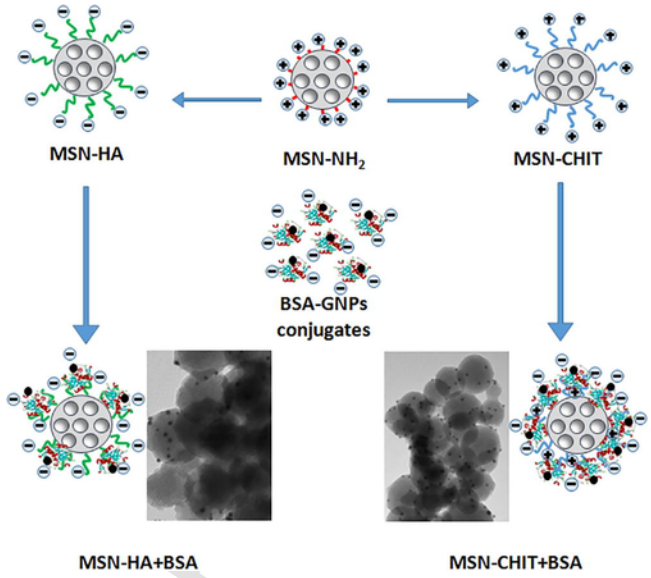

Scheme 1. Direct visualization of BSA-GNP conjugates on the surface of biopolymer-modified MSNs (MSN-HA and MSN-CHIT).

2. Materials and methods

2.1. Chemicals

Tetraethoxysilane (TEOS, 98%), hexadecyltrimethylammonium bromide (CTAB, > 99%), anhydrous toluene (99.8%), 3-aminopropyl-triethoxysilane (APTES, > 98%), triethylamine (> 99%), hyaluronic acid (MW = 90–130 kDa), chitosan (cod. 740,063, MW = 60–120 kDa), NaH_2PO_4 (99%), Na_2HPO_4 (99%), hydrochloride acid (37%), and glutaraldehyde (50% aqueous solution) were purchased from Sigma-Aldrich (Milan, Italy). *N*-hydroxysuccinimide (NHS, > 97%), and *N*-(3-dimethylaminopropyl)-*N*′-ethylcarbodiimide hydrochloride (EDC, > 98%) were purchased from Fluka. Bovine serum albumin conjugated with gold nanoparticles (BSA-GNPs) was purchased from British BioCell International.

2.2. Synthesis and functionalization of MSNs with HA and CHIT biopolymers

MSNs were synthesized by a silica precursor (TEOS) and an organic surfactant (CTAB) as reported in ref.s [25,32]. After surfactant removal MSNs were functionalized with APTES (0.5 mL for 1 g of MSNs) with a post-synthesis functionalization [25,32]. The resulting MSN-NH_2 sample was collected by filtration, washed with toluene and acetone, and dried overnight at room temperature under vacuum. HA-grafted MSNs (MSN-HA) were synthesized as described in ref. [32]. Briefly, an aqueous solution of NHS (0.186 g), EDC (0.113 g) and HA (0.060 g) was added to a dispersion of 0.5 g of MSN-NH_2 in water. The pH was adjusted to 9.0 by adding triethylamine and the mixture was stirred at 38 °C overnight. The obtained white powder was centrifuged, washed with water, and dried under vacuum and at room temperature overnight. CHIT-grafting was carried out as reported in ref. [32], by adding to a dispersion of 0.5 g of MSN-NH_2 at pH = 7.5 1 mL of aqueous glutaraldehyde (50%). Then, the obtained red powder was dispersed in an aqueous solution containing chitosan (0.055 g) and HCl 0.1 M to promote the solubilization of the biopolymer. The obtained MSN-CHIT was collected by centrifugation, washed with a basic buffer solution (pH = 8), and dried overnight under vacuum at room temperature.

2.3. Adsorption of bovine serum albumin (BSA)

2.3.1. Adsorption of BSA on MSNs

A mass of 25 mg of MSNs previously functionalized (MSN-NH_2, MSN-HA or MSN-CHIT) was suspended in 5 mL of a 20 mg/mL solution of BSA in 10 mM phosphate buffer saline (PBS) solution (pH = 7.4 and 0.15 M NaCl) for 24 h at 25 °C. The powder was centrifuged, washed with PBS for three times and dried under vacuum at room temperature overnight. These BSA-loaded materials (MSN-NH_2, MSN-HA and MSN-CHIT + BSA) were submitted to FTIR, TGA and light scattering characterization.

2.3.2. Adsorption of BSA-GNPs on MSNs

A mass of 5 mg of MSNs previously functionalized (MSN-NH_2, MSN-HA or MSN-CHIT) was suspended in 100 μL of BSA-GNPs and 100 μL of 10 mM PBS solution (pH = 7.4 and 0.15 M NaCl) and left under agitation for 2 h at 25 °C. After supernatant removal the powder was suspended in 100 μL of fresh PBS and 50 μL of glutaraldehyde 50% w/w for fixing the protein to MSNs. The suspension was gently stirred for another hour at 25 °C. The obtained red powder was centrifuged, washed with PBS and dried overnight under vacuum at room temperature [58]. BSA-GNPs loaded samples were then used for TEM analysis.

2.4. Characterization of functionalized MSNs

The textural characterization was carried out on an ASAP 2020 instrument, by determining the N_2 adsorption/desorption isotherm at 77 K. Before analysis MSN-NH_2 samples was heated at 110 °C at a rate of 1 °C/min under vacuum for 24 h, whereas polymer-functionalized sample (MSN-HA and MSN-CHIT) were outgassed under the same conditions while heating at 40 °C for 60 h. The hexagonal structure was determined by small-angle X-rays scattering (SAXS) analysis. Patterns were recorded for 1 h with a S3-MICRO SWAXS camera system (HECUS X-ray Systems, Graz, Austria). CuKα radiation of wavelength 1.542 Å was provided by a Genix X-ray generator, operating at 30 kV and 0.4 mA.

Transmission electron microscopy (TEM) analysis was carried out placing appropriate amounts of finely ground powder samples onto carbon-coated copper grids that were observed and photographed by a Hitachi H-7000 microscope equipped with a thermionic gun operating at 100 kV. Digital images were acquired by an AMT DVC CCD camera.

Thermogravimetric analysis (TGA) was carried out on a Mettler-Toledo TGA/STDA 851. Thermal analysis data were collected in the 25–1000 °C range, under oxygen flow (heating rate = 10 °C·min^{-1}; flow rate = 50 mL·min^{-1}) using argon as the carrier.

The hydrodynamic diameter and the zeta potential of MSNs were measured using a Zetasizer nano ZSP (Malvern Instruments) in backscatter configuration (θ = 173°) at laser wavelength of λ = 633 nm. The scattering cell temperature was fixed at 37 °C and the data were analysed with the Zetasizer software 7.03 version. For both zeta potential and hydrodynamic diameter measurements the samples were prepared by suspending MSNs (1 mg/mL) in filtered (0.2 μm polypropylene filter, Whatman) millipore water. Before measurements the samples were left under agitation overnight and sonicated for 30 min.

The surface functionalization was confirmed through Fourier transform infrared (FTIR) studies conducted with a Bruker Tensor 27 spectrophotometer equipped with a diamond-ATR accessory and a DTGS detector. A number of 256 scans at a resolution of 2 cm^{-1} were averaged in the spectral range 4000 cm^{-1}–400 cm^{-1}.

3. Results and discussion

3.1. Characterization of MSNs

The synthesized MSNs were initially functionalized with APTES to obtain MSN-NH_2, and then with hyaluronic acid (HA) and chitosan (CHIT) biopolymers obtaining MSN-HA and MSN-CHIT samples. The samples were then characterized through different physico-chemical techniques. Fig. 1A shows nitrogen adsorption/desorption isotherms. All samples exhibit a typical type IV isotherm with a small hysteresis cycle at $p/p^\circ > 0.9$ due to the capillary condensation of nitrogen into the mesopores. Table 1 reports the textural parameters: the surface area was calculated through the BET method (S_{BET}) [25,59], whereas the pore size distributions were obtained by the BJH method [25,60]. The hysteresis of the functionalized samples lies at lower adsorbed nitrogen volumes than the original MSNs, due to a decrease of pore volume induced by the functionalization. This is paralleled by the decrease of the pore size as shown in Fig. 1B. SAXS patterns (Fig. 1C) show for all samples an intense peak, due to the reflection of (1 0 0) plane, and two weak peaks due to the reflection of (1 1 0) and (2 0 0) planes respectively. These patterns are associated to materials with a hexagonal array of pores. The lattice parameters, *a,* shown in Table 1, confirm that both the amino- and the polymer-functionalization do not alter the ordered structure of the MSNs. TEM micrograph for MSN-NH_2 (Fig. 1D) shows almost spherical nanoparticles with size in the range 80–130 nm, and confirms the occurrence of an ordered hexagonal array of pores. The hydrodynamic diameter (d_H) of MSNs samples dispersed in distilled water at 37 °C was measured through dynamic light scattering (DLS). The d_H values obtained for the different MSN samples, reported in Table 1, are in agreement with TEM data.

FTIR spectra (Fig. 2) show the characteristic peaks of silica materials for all samples. That is, two intense peaks at 1070 cm^{-1} and 795 cm^{-1} attributed to the asymmetric and symmetric stretching vibration of Si-O-Si, respectively. Other two peaks at 965 cm^{-1} and 450 cm^{-1} are related to Si-OH bending and to the deformation modes of the O-Si-O, respectively. MSN-NH_2 spectrum shows an additional peak at 1547 cm^{-1} due to the asymmetric –NH_2 bending, which confirms the amino-functionalization. MSN-HA sample displays a peak at 1636 cm^{-1} assigned to C = O stretching [40,61]. Finally, MSN-CHIT spectrum shows two peaks at 1649 cm^{-1} and 1556 cm^{-1} due to C = N stretching and the asymmetric bending of amino groups in the biopolymer chain [61].

Thermogravimetric analysis (TGA) was then carried out. Fig. 3 shows the graphs of mass loss (Δm %) as a function of temperature for the original and the functionalized MSN samples. At temperatures below 200 °C the mass loss can be ascribed to the removal of humidity and to the condensation of surface silanols. Above 200 °C, Δm values can be directly related to the extent of surface functionalization.

The mass loss values are reported in Table 2. Remarkably, the similar Δm % values obtained for MSN-HA and MSN-CHIT samples suggest that a similar degree of biopolymer functionalization was achieved. Electrophoretic light scattering measurements in distilled water result in a different surface potential depending on surface functionalization. Zeta potential (ζ) values are strongly negative for pure silica (−20.0 mV) and become positive after amino-functionalization (+30.6 mV). Likewise, ζ values for MSN-HA and MSN-CHIT are negative and positive, due to the occurrence of dissociated carboxylic groups of hyaluronic acid and protonated amino groups of chitosan chains, respectively. An additional evidence of surface functionalization is provided by the increase of hydrodynamic diameter (d_H) for the functionalized MSNs, as reported in Table 1.

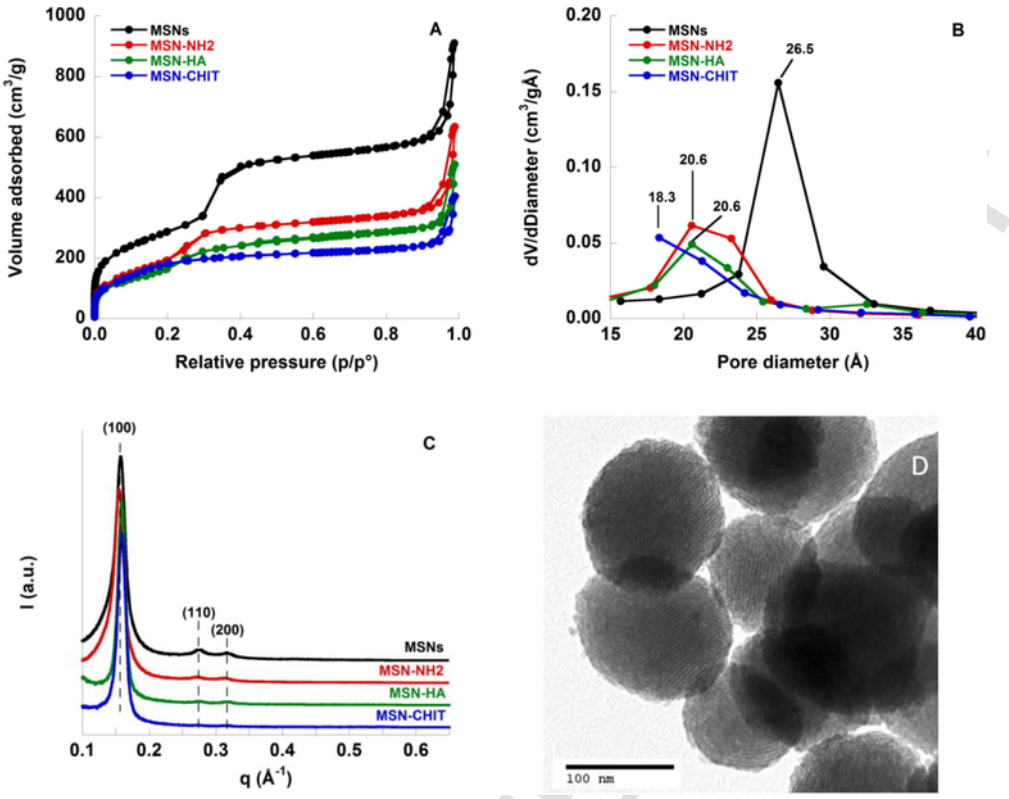

Fig. 1. Characterization of MSNs (black), MSN-NH_2 (red), MSN-HA (green), and MSN-CHIT (blue) samples: (A) adsorption/desorption N_2 isotherms; (B) pore size distribution; (C) SAXS patterns. (D) TEM micrograph of MSN-NH_2 sample.

Table 1
Surface area (S_{BET}), pore diameter (d_{BJH}), pore volume (V_p), and lattice parameter (a) and hydrodynamic diameter (d_H) in distilled water at 37 °C of MSNs.

Sample	[a]S_{BET} (m^2/g)	[b]$d_{Des,BJH}$ (Å)	[c]$V_{pDes,BJH}$ (cm^3/g)	[d]a (Å)	[e]d_H (nm)
MSN	1061	26.5	1.41	45.4	140 ± 12
MSN-NH_2	894	20.6	0.98	45.9	160 ± 6
MSN-HA	735	20.6	0.79	45.4	168 ± 11
MSN-CHIT	623	18.3	0.63	45.4	186 ± 7

[a] Surface area calculated by the BET method.
[b] Pore diameter from desorption branch calculated by BJH method.
[c] Pore volume calculated at p/p° = 0.99.
[d] Lattice parameter obtained by SAXS.
[e] Hydrodynamic diameter obtained by DLS.

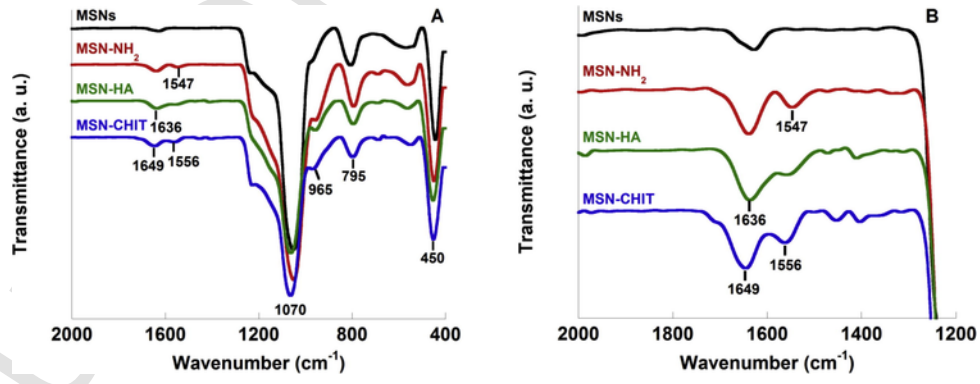

Fig. 2. FTIR spectra of original and functionalized MSN samples.

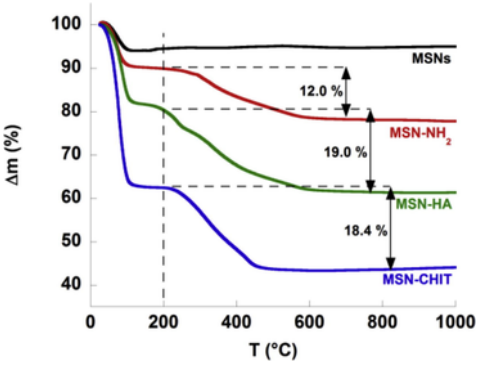

Fig. 3. Thermogravimentric analysis (TGA) of MSNs, MSN-NH_2, MSN-HA and MSN-CHIT samples.

Table 2
Characterization of biopolymer-functionalized MSNs and BSA-loaded MSNs. Percentage mass loss (Δm) below and above 200 °C. Zeta potential (ζ) and hydrodynamic diameter (d_H) in distilled water at 37 °C. Loading of BSA (L_{BSA}).

Sample	Δm (%)		ζ (mV)	L_{BSA} (mg/g)
	< 200 °C	> 200 °C		
MSN	7.6	4.0	−20.0 ± 0.2	–
MSN-NH_2	10.2	12.0	+30.6 ± 0.5	–
MSN-HA	19.6	19.0	−14.8 ± 0.9	–
MSN-CHIT	37.6	18.4	+10.1 ± 0.3	–
MSN-NH_2 + BSA	11.4	18.1	+9.3 ± 0.3	65
MSN-HA + BSA	15.2	26.3	−18.5 ± 0.4	79
MSN-CHIT + BSA	11.9	29.7	−7.7 ± 0.6	127

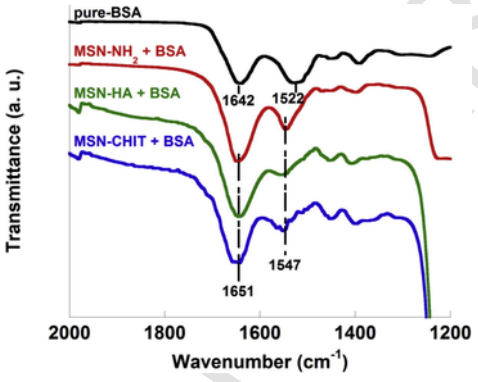

Fig. 4. FTIR spectra of Functionalized MSNs loaded with BSA.

3.2. Adsorption of BSA on biopolymer-modified MSNs

The biopolymer-functionalized materials were then suspended in a 20 mg/mL BSA solution in PBS (pH 7.4, NaCl 150 mM) to simulate the formation of the protein corona in physiological systems [57,62]. In order to evaluate the extent of BSA adsorption on the surface of the biopolymer-functionalized materials, MSN-NH_2 + BSA, MSN-HA + BSA and MSN-CHIT + BSA samples were characterized through FTIR, TGA and electrophoretic light scattering (ELS) measurements. Fig. 4 shows FTIR spectra of pure BSA and BSA-loaded MSNs (MSN-HA + BSA and MSN-CHIT + BSA). The FTIR spectrum of BSA protein displays two characteristic bands at 1642 cm^{-1} and 1522 cm^{-1} named amide I (C = O stretching) and amide II (C-N stretching and N-H bending), respectively [63–65]. The occurrence of these two characteristic bands proves the successful adsorption of a protein on a solid support [19,66,67]. In Fig. 4 we observe two bands at 1651 cm^{-1} and 1547 cm^{-1} in the pure-BSA sample. In the FTIR spectra of MSN-BSA samples, it is difficult to assign univocally those bands to amide I and amide II due to the occurrence of vibrations of the functional groups of HA and CHIT biopolymers grafted on MSNs in the same spectral region (compare Figs. 2 and 4). It is likely that for MSN-HA + BSA and MSN-CHIT + BSA samples those bands are overlapped, preventing therefore unambiguous peak assignment.

However, BSA adsorption on biopolymer-functionalized MSNs can be assessed by TGA measurements shown in Fig. 5A-C. For all samples an increase of Δm (%) after BSA adsorption is observed (Table 2). These values are higher for biopolymer-functionalized materials, MSN-HA (26.3%) and MSN-CHIT (29.7%) than for the amino-functionalized MSN-NH_2 (18.1%). The corresponding values of BSA loading (L_{BSA}), calculated from Δm (%) values, are L_{BSA} = 65 mg/g, 79 mg/g, and 127 mg/g for MSN-NH_2, MSN-HA and MSN-CHIT, respectively. These results confirm that BSA protein is effectively adsorbed on MSNs surface and that, under our experimental conditions (pH 7.4, ionic strength 0.15 M, T = 37 °C), the type of functionalization modulates the amount of adsorbed BSA. Indeed, the amount of BSA loading is in the order MSN-CHIT > MSN-HA > MSN-NH_2.

These trends can be interpreted by taking into account the different electrical charge carried by the biopolymers and the protein. Indeed under our adsorption conditions (PBS pH = 7.4 and 0.15 M NaCl) MSN-HA sample is negatively charged due the dissociation of carboxylic groups occurring in the HA chains. On the contrary, amino groups of CHIT biopolymer are protonated, and thus positively charged. Furthermore, in the same physiological conditions, BSA has a net negative charge since its isoelectric point (IEP) is about 4.7 [68,69]. Assuming that only the electrostatic interaction is operating, we would expect a high BSA loading for MSN-CHIT and a negligible or low BSA loading for MSN-HA. BSA loading indeed decreases in the order MSN-CHIT > MSN-HA > MSN-NH_2. The non-negligible BSA loading recorded on MSN-HA, however, suggests that electrostatics is likely not the only interaction at work. Once BSA has been adsorbed on the MSNs surface,

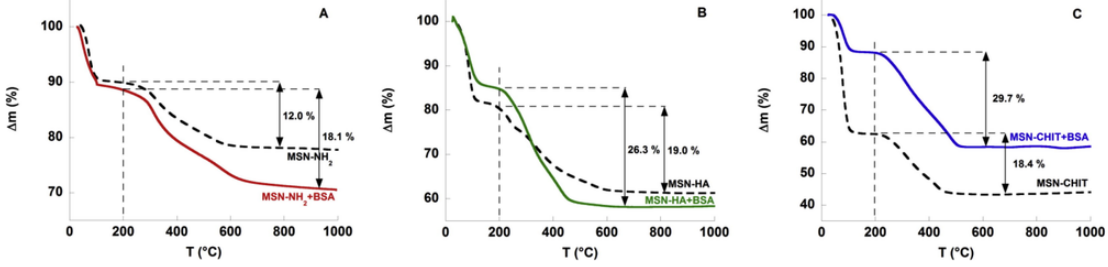

Fig. 5. Percentage mass loss profiles as a function of temperature for MSN-NH_2 (A), MSN-HA (B) and MSN-CHIT (C) and the corresponding BSA-loaded samples as determined by TGA.

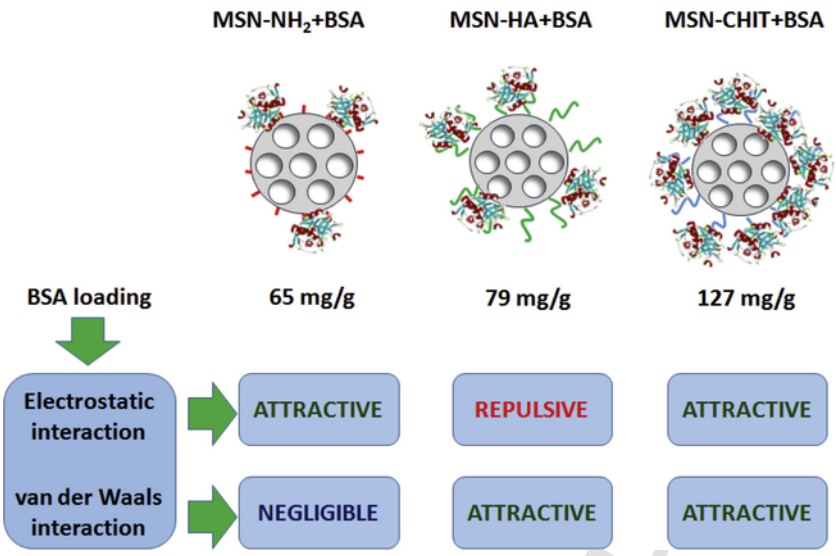

Scheme 2. Interactions responsible of the formation of the protein corona on functionalized MSNs.

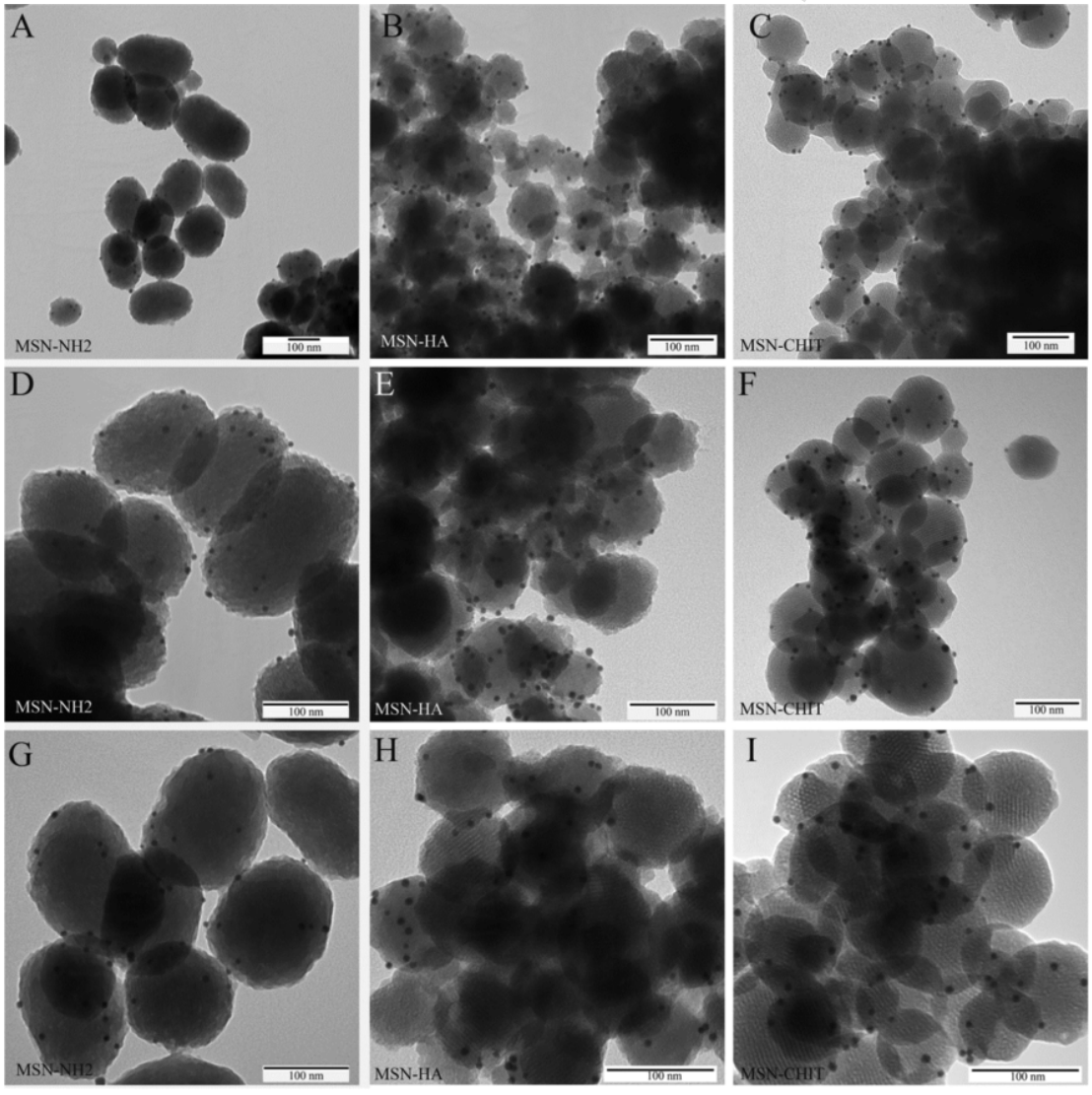

Fig. 6. TEM micrographs of MSN-NH_2 + BSA-GNPs (A, D, G) MSN-HA + BSA-GNPs (B, E, H) and MSN-CHIT + BSA-GNPs (C, F , I).

it changes the physico-chemical features of the NPs [11], as demonstrated by electrophoretic light scattering results reported in Table 2. Indeed, ζ-potential values for all samples are strongly affected by the presence of adsorbed BSA molecules. In particular, we observe a decrease of ζ values for MSN-NH_2 – from +30.6 to +9.3 mV – and a charge reversal for MSN-CHIT from +10.1 mV to −7.7 mV. This can be explained by a strong interaction between the negatively charged BSA and the positively charged particles, in our adsorption conditions. In the case of MSN-HA we observed a slightly more negative value of ζ from −14.8 mV to −18.5 mV. Such a change of ζ value is consistent with the adsorption of negatively charged BSA molecules on the negatively charged MSN-HA particles, as already confirmed by TGA data. Although the attraction of two species with like charges might sound counterintuitive, it should be recalled that BSA adsorption might take place on positively charged patches occurring also above its IEP [70]. Moreover, we should also consider that under physiological conditions electrostatics is screened. It is easy to calculate that at a 100 mM NaCl concentration the Debye length is about 1 nm. This means that a surface potential of 100 mV is reduced by charge screening to about 5–10 mV within the diffuse layer. Hence, above 100 mM salt concentration the intensity of the electrostatic force is comparable to that of non-electrostatic van der Waals interactions [71]. Therefore, due to electrolyte-induced surface potential screening, the ubiquitous attractive van der Waals forces between uncharged BSA and hyaluronic patches is likely responsible of the BSA loading of 79 mg/g. The fact that besides electrostatics also other interactions are operating is demonstrated by the lower BSA loading (65 mg/g) reached by the positively charged MSN-NH_2 (Scheme 2).

What obtained here seems to confirm the findings observed in a previous work where the internalization of functionalized MSNs on 3T3 mouse fibroblast cells was investigated [32]. Indeed, in the protein-rich cell culture medium MSN-NH_2 and MSN-HA particles were easily internalized whereas MSN-CHIT resulted in the formation of large aggregates which could not be internalized by 3T3 cells. The high BSA loading on MSN-CHIT, obtained by TGA measurements, is consistent with the drastic change of zeta potential (Table 2) which is likely the cause of the formation of those particle aggregates [32].

3.3. Transmission electron microscopy analysis

TEM characterization was used to highlight the inner mesoporous structure of all samples and confirm BSA adsorption on surfaces of most of MSN samples examined in this investigation. In detail, in order to detect the presence of BSA on the MSNs, we used a specific gold labelling technique that consisted mainly of BSA conjugated with gold nanoparticles (GNPs). The use of GNP-antibody conjugates was previously used to localize human lysozyme [72] and an antibody fragment [58] within the pores of SBA-15 mesoporous silica. Here, the BSA-GNPs conjugates allowed the visualization of BSA adsorbed on MSNs. Both MSN-HA and MSN-CHIT samples showed similar BSA-GNPs patterns that were mainly characterized by the presence of an evident and intense gold labelling decorating the MSN surfaces (Fig. 6). However, variability of gold labelling intensity was occasionally observed. Overall, by a careful examination of several samples, a qualitative higher abundance of gold labelling was observed for MSN-CHIT than for MSN-HA in agreement with TGA data. The lower abundance of gold labelling for MSN-NH_2 sample is also in qualitative agreement with the lowest BSA loading, quantified through TGA (Table 2).

4. Conclusions

Taking into consideration the results of this study we can remark that the choice of a simple model provided interesting information on the interaction between BSA and functionalized MSNs. Our system was constituted by HA/CHIT-functionalized MSNs suspended in a 20 mg/mL BSA aqueous solution (phosphate buffer solution at pH 7.4 and NaCl 150 mM) at T = 37 °C. Within these conditions BSA interacts with the MSNs surface covered by the biopolymer. BSA is able to interact with both types of sample even though they carry opposite electric charges. This is an additional proof of the importance of non-electrostatic van der Waals interactions particularly in biological systems [71]. In fact, electrostatic and non electrostatic interactions likely cooperate to get the highest BSA loading on MSN-CHIT sample. For MSN-HA, instead, the two types of interactions have opposite effects which, nonetheless, overall result in a relatively high BSA loading. The effective adsorption of BSA is clearly demonstrated by TEM images of the samples treated with a GNP labelling procedure. Once BSA covers functionalized MSNs surface, the resulting surface potential is quite different from that of bare particles. That is a relevant finding which can influence the formation of the protein corona, and results in a different destiny of functionalized MSNs, once dispersed in a cellular medium or in a body fluid.

Acknowledgments

Financial support from FIR 2017, RAS/FdS (CUP F72F16003070002, 2017) European Research Council (Advanced Grant VERDI; ERC-2015-AdG Proposal N. 694160 is gratefully acknowledged.

References

[1] J. Zhang, Y. Sun, B. Tian, K. Li, L. Wang, Y. Liang, J. Han, Multifunctional mesoporous silica nanoparticles modified with tumor-shedable hyaluronic acid as carriers for doxorubicin, Colloids Surfaces. B 144 (2016) 293–302, https://doi.org/10.1016/j.colsurfb.2016.04.015.

[2] S. Baek, R. Singh, D. Khanal, K.D. Patel, E.-J. Lee, K.W. Leong, W. Chrzanowski, H.-W. Kim, Smart multifunctional drug delivery towards anticancer therapy harmonized in mesoporous nanoparticles, Nanoscale 7 (2015) 14191–14216, https://doi.org/10.1039/C5NR02730F.

[3] V. Keskar, P.S. Mohanty, E.J. Gemeinhart, R.A. Gemeinhart, Cervical cancer treatment with a locally insertable controlled release delivery system, J. Control Release 115 (2006) 280–288, https://doi.org/10.1016/j.jconrel.2006.08.014.

[4] P. Nittayacharn, N. Nasongkla, Development of self-forming doxorubicin-loaded polymeric depots as an injectable drug delivery system for liver cancer chemotherapy, J. Mater. Sci. – Mater. Med. 28 (2017) 101–113, https://doi.org/10.1007/s10856-017-5905-8.

[5] C. Monterrubio, G. Pascual-Pasto, F. Cano, M. Vila-Ubach, A. Manzanares, P. Schaiquevich, J.A. Tornero, A. Sosnik, J. Mora, A.M. Carcaboso, SN-38-loaded nanofiber matrices for local control of pediatric solid tumors after subtotal resection surgery, Biomaterials 79 (2016) 69–78, https://doi.org/10.1016/j.biomaterials.2015.11.055.

[6] M. Norouzi, B. Nazari, D.W. Miller, Injectable hydrogel-based drug delivery systems for local cancer therapy, Drug Discovery Today 21 (2016) 1835–1849, https://doi.org/10.1016/j.drudis.2016.07.006.

[7] A. Di Martino, O.A. Guselnikova, M.E. Trusova, P.S. Postnikov, V. Sedlarik, Organic-inorganic hybrid nanoparticles controlled delivery system for anticancer drugs, Int. J. Pharm. 526 (2017) 380–390, https://doi.org/10.1016/j.ijpharm.2017.04.061.

[8] C. Ding, Z. Li, A review of drug release mechanisms from nanocarrier systems, Mater. Sci. Eng., C 76 (2017) 1440–1453, https://doi.org/10.1016/j.msec.2017.03.130.

[9] Q. Zhang, Z. Wu, N. Li, Y. Pu, B. Wang, T. Zhang, J. Tao, Advanced review of graphene-based nanomaterials in drug delivery systems: synthesis, modification, toxicity and application, Mater. Sci. Eng., C 77 (2017) 1363–1375, https://doi.org/10.1016/j.msec.2017.03.196.

[10] M. Bikram, A.M. Gobin, R.E. Whitmire, J.L. West, Temperature-sensitive hydrogels with SiO2-Au nanoshells for controlled drug delivery, J. Control. Release 123 (2007) 219–227, https://doi.org/10.1016/j.jconrel.2007.08.013.

[11] G. Villaverde, A. Baeza, G.J. Melen, A. Alfranca, M. Ramirez, M. Vallet-Regí, A new targeting agent for the selective drug delivery of nanocarriers for treating neuroblastoma, J. Mater. Chem. B. 3 (2015) 4831–4842, https://doi.org/10.1039/C5TB00287G.

[12] J. Jiao, X. Li, S. Zhang, J. Liu, D. Di, Y. Zhang, Q. Zhao, S. Wang, Redox and pH dual-responsive PEG and chitosan-conjugated hollow mesoporous silica for controlled drug release, Mater. Sci. Eng., C 67 (2016) 26–33, https://doi.org/10.1016/j.msec.2016.04.091.

[13] M. Monduzzi, S. Lampis, S. Murgia, A. Salis, From self-assembly fundamental knowledge to nanomedicine developments, Adv. Colloid Interface Sci. 205 (2014) 48–67, https://doi.org/10.1016/j.cis.2013.10.009.

[14] C.T. Kresge, M.E. Leonowicz, W.J. Roth, J.C. Vartuli, J.S. Beck, Ordered mesoporous molecular sieves synthesized by liquid-crystal template mechanism, Nature 359 (1992) 710–712, https://doi.org/10.1038/355242a0.

[15] M. Vallet-Regi, A. Rámila, R.P. Del Real, J. Pérez-Pariente, A new property of MCM-41: Drug delivery system, Chem. Mater. 13 (2001) 308–311, https://doi.org/10.1021/cm0011559.

[16] M. Vallet-Regì, J.C. Doadrio, A.L. Doadrio, I. Izquierdo-Barba, J. Perez-Pariente, Hexagonal ordered mesoporous material as a matrix for the controlled release of amoxicillin, Solid State Ionics 172 (2004) 435–439, https://doi.org/10.1016/j.ssi.2004.04.036.

[17] D. Molina-Manso, M. Manzano, J.C. Doadrio, G. Del Prado, A. Ortiz-Pérez, M. Vallet-Regì, E. Gòmez-Barrena, J. Esteban, Usefulness of SBA-15 mesoporous ceramics as a delivery system for vancomycin, rifampicin and linezolid: a preliminary report, Int. J. Antimicrob. Agents 40 (2012) 252–256, https://doi.org/10.1016/j.ijantimicag.2012.05.013.

[18] N. Gómez-Cerezo, I. Izquierdo-Barba, D. Arcos, M. Vallet-Regí, Tailoring the biological response of mesoporous bioactive materials, J. Mater. Chem. B. 3 (2015) 3810–3819, https://doi.org/10.1039/C5TB00268K.

[19] M.S. Bhattacharyya, P. Hiwale, M. Piras, L. Medda, D. Steri, M. Piludu, A. Salis, M. Monduzzi, Lysozyme adsorption and release from ordered mesoporous materials, J. Phys. Chem. C. 114 (2010) 19928–19934, https://doi.org/10.1021/jp1078218.

[20] D. Steri, M. Monduzzi, A. Salis, Ionic strength affects lysozyme adsorption and release from SBA-15 mesoporous silica, Microporous Mesoporous Mater. 170 (2013) 164–172, https://doi.org/10.1016/j.micromeso.2012.12.002.

[21] R.R. Castillo, A. Baeza, M. Vallet-Regí, Recent applications of the combination of mesoporous silica nanoparticles with nucleic acids: development of bioresponsive devices, carriers and sensors, Biomater. Sci. 5 (2017) 353–377, https://doi.org/10.1039/C6BM00872K.

[22] R.R. Castillo, M. Colilla, M. Vallet-Regí, Advances in mesoporous silica-based nanocarriers for co-delivery and combination therapy against cancer, Expert Opin. Drug Delivery. 14 (2017) 229–243, https://doi.org/10.1080/17425247.2016.1211637.

[23] S. Rahmani, J.O. Durand, C. Charnay, L. Lichon, M. Férid, M. Garcia, M. Gary-Bobo, Synthesis of mesoporous silica nanoparticles and nanorods: Application to doxorubicin delivery, Solid State Sci. 68 (2017) 25–31, https://doi.org/10.1016/j.solidstatesciences.2017.04.003.

[24] J.L. Paris, M.V. Cabanas, M. Manzano, M. Vallet-Regí, Polymer-grafted mesoporous silica nanoparticles as ultrasound-responsive drug carriers, ACS Nano 9 (2015) 11023–11033, https://doi.org/10.1021/acsnano.5b04378.

[25] V. Nairi, L. Medda, M. Monduzzi, A. Salis, Adsorption and release of ampicillin antibiotic from ordered mesoporous silica, J. Colloid Interface Sci. 497 (2017) 217–225, https://doi.org/10.1016/j.jcis.2017.03.021.

[26] F. Sevimli, A. Yılmaz, Surface functionalization of SBA-15 particles for amoxicillin delivery, Microporous Mesoporous Mater. 158 (2012) 281–291, https://doi.org/10.1016/j.micromeso.2012.02.037.

[27] W. Fang, Z. Wang, S. Zong, H. Chen, D. Zhu, Y. Zhong, Y. Cui, Biosensors and Bioelectronics pH-controllable drug carrier with SERS activity for targeting cancer cells, Biosens. Bioelectron. 57 (2014) 10–15, https://doi.org/10.1016/j.bios.2014.01.042.

[28] D.P. Ferris, J. Lu, C. Gothard, R. Yanes, C.R. Thomas, J. Olsen, J.F. Stoddart, F. Tamanoi, J.I. Zink, Synthesis of Biomolecule-Modifi ed Mesoporous Silica Nanoparticles for Targeted Hydrophobic Drug Delivery to, Cancer Cells (2011) 1816–1826, https://doi.org/10.1002/smll.201002300.

[29] K. Cheng, S.R. Blumen, M.B. Macpherson, J.L. Steinbacher, B.T. Mossman, C.C. Landry, Enhanced uptake of porous silica microparticles by bifunctional surface biocompatible, Polymer 2 (2010) 2489–2495, https://doi.org/10.1021/am100530t.

[30] Z.-Y. Li, J.-J. Hu, Q. Xu, S. Chen, H. Jia, Y.-X. Sun, R.-X. Zhuo, X.-Z. Zhang, A redox-responsive drug delivery system based on RGD containing peptide-capped mesoporous silica, J. Mater. Chem. B 3 (2015) 39–44, https://doi.org/10.1039/C4TB01533A.

[31] J. Zhang, Z.-F. Yuan, Y. Wang, W.-H. Chen, G.-F. Luo, S.-X. Cheng, R. Zhuo, X. Zhang, Multifunctional envelope-type mesoporous silica nanoparticles for tumor-triggered targeting drug delivery, J. Am. Chem. Soc. 135 (2013) 5068–5073, do: /10.1021/ja312004m.

[32] A. Salis, M. Fanti, L. Medda, V. Nairi, F. Cugia, M. Piludu, V. Sogos, M. Monduzzi, Mesoporous silica nanoparticles functionalized with hyaluronic acid and chitosan biopolymers. effect of functionalization on cell internalization, ACS Biomater. Sci. Eng. 2 (2016) 741–751, https://doi.org/10.1021/acsbiomaterials.5b00502.

[33] A. Popat, J. Liu, G.Q. (Max) Lu, S.Z. Qiao, A pH-responsive drug delivery system based on chitosan coated mesoporous silica nanoparticles, J. Mater. Chem. 22 (2012) 11173–11178, https://doi.org/10.1039/c2jm30501a.

[34] W.T. Liu, Y. Yang, P.H. Shen, X.J. Gao, S.Q. He, H. Liu, C.S. Zhu, Facile and simple preparation of pH-sensitive chitosan-mesoporous silica nanoparticles for future breast cancer treatment, Express Polym. Lett. 9 (2015) 1068–1075, https://doi.org/10.3144/expresspolymlett.2015.96.

[35] G. Villaverde, V. Nairi, A. Baeza, M. Vallet-Regí, Double sequential encrypted targeting sequence: a new concept for bone cancer treatment, Chem. – A Eur. J. 23 (2017) 7174–7179, https://doi.org/10.1002/chem.201605947.

[36] Z. Wang, Y. Tian, H. Zhang, Y. Qin, D. Li, L. Gan, F. Wu, Using hyaluronic acid-functionalized pH stimuli-responsive mesoporous silica nanoparticles for targeted delivery to CD44-overexpressing cancer cells, Int. J. Nanomed. 11 (2016) 6485–6497, https://doi.org/10.2147/IJN.S117184.

[37] M. Chang, F. Zhang, T. Wei, T. Zuo, Y. Guan, G. Lin, W. Shao, Smart linkers in polymer-drug conjugates for tumor-targeted delivery, J. Drug Target. 24 (2016) 475–491, https://doi.org/10.3109/1061186X.2015.1108324.

[38] A. Baeza, M. Colilla, M. Vallet-Regí, Advances in mesoporous silica nanoparticles for targeted stimuli-responsive drug delivery, Expert Opin. Drug Delivery 12 (2015) 319–337, https://doi.org/10.1517/17425247.2014.953051.

[39] G. Li, Y. Gao, Y. Cui, T. Zhang, R. Cui, Y. Jiang, J. Shi, Overexpression of CD44 is associated with the occurrence and migration of non-small cell lung cancer, Mol. Med. Rep. 14 (2016) 3159–3167, https://doi.org/10.3892/mmr.2016.5636.

[40] L. Medda, M.F. Casula, M. Monduzzi, A. Salis, Adsorption of lysozyme on hyaluronic acid functionalized SBA-15 mesoporous silica: a possible bioadhesive depot system, Langmuir 43 (2014) 12996–13004, https://doi.org/10.1021/la503224n.

[41] Y. Wang, Q. Zhao, N. Han, L. Bai, J. Li, J. Liu, E. Che, L. Hu, Q. Zhang, T. Jiang, S. Wang, Mesoporous silica nanoparticles in drug delivery and biomedical applications, Nanomedicine: Nanotechnology, Biol. Med. 11 (2015) 313–327, https://doi.org/10.1016/j.nano.2014.09.014.

[42] J. Liu, Y. Huang, A. Kumar, A. Tan, S. Jin, A. Mozhi, X.J. Liang, PH-Sensitive nano-systems for drug delivery in cancer therapy, Biotechnol. Adv. 32 (2014) 693–710, https://doi.org/10.1016/j.biotechadv.2013.11.009.

[43] L. Treuel, G.U. Nienhaus, Toward a molecular understanding of nanoparticle-protein interactions, Biophys. Rev. 4 (2012) 137–147, https://doi.org/10.1007/s12551-012-0072-0.

[44] S. Laurent, C. Burtea, C. Thirifays, F. Rezaee, M. Mahmoudi, Significance of cell "observer" and protein source in nanobiosciences, J. Colloid Interface Sci. 392 (2013) 431–445, https://doi.org/10.1016/j.jcis.2012.10.005.

[45] M. Mahmoudi, I. Lynch, M.R. Ejtehadi, M.P. Monopoli, F.B. Bombelli, S. Laurent, Protein − nanoparticle interactions: opportunities and challenges, Chem. Rev. 111 (2011) 5610–5637, https://doi.org/10.1021/cr100440g.

[46] Z. Deng, G. Mortimer, T. Schiller, A. Masumeci, D. Martin, M. RF, Differential plasma protein binding to metal oxide nanoparticles, Nanotechnology 20 (2009) 455101–455109, https://doi.org/10.1088/0957-4484/20/45/455101.

[47] S. Tenzer, D. Docter, S. Rosfa, A. Wlodarski, J. Kuharev, A. Rekik, S.K. Knauer, C. Bantz, T. Nawroth, C. Bier, J. Sirirattanapan, W. Mann, L. Treuel, R. Zellner, M. Maskos, H. Schild, R.H. Stauber, Nanoparticle size is a critical physicochemical determinant of the human blood plasma corona: a comprehensive quantitative proteomic analysis, ACS Nano 5 (2011) 7155–7167, https://doi.org/10.1021/nn201950e.

[48] M.C. Cox, K.J. Barnham, T.A. Frenkiel, J.D. Hoeschele, A.B. Mason, Q.Y. He, R.C. Woodworth, P.J. Sadler, Identification of platination sites on human serum transferrin using (13)C and (15)N NMR spectroscopy., Journal of Biological Inorganic Chemistry : JBIC : A Publication of the Society of Biological, Inorg. Chem. 4 (1999) 621–631.

[49] P. Aggarwal, J.B. Hall, C.B. McLeland, M.A. Dobrovolskaia, S.E. McNeil, Nanoparticle interaction with plasma proteins as it relates to particle biodistribution, biocompatibility and therapeutic efficacy, Adv. Drug Deliv. Rev. 61 (2009) 428–437, https://doi.org/10.1016/j.addr.2009.03.009.

[50] S. Laurent, M. Mahmoudi, Superparamagnetic iron oxide nanoparticles: Promises for diagnosis and treatment of cancer, Int. J. Mol. Epidemiol. Genet. 2 (2011) 367–390, https://doi.org/10.1021/cn100100e.

[51] I. Lynch, K.A. Dawson, Protein-nanoparticle interactions, Nano Today 3 (2008) 40–47, https://doi.org/10.1016/S1748-0132(08)70014-8.

[52] P. Foroozandeh, A.A. Aziz, Merging worlds of nanomaterials and biological environment: factors governing protein corona formation on nanoparticles and its biological consequences, Nanoscale Res. Lett. 10 (2015) 221–232, https://doi.org/10.1186/s11671-015-0922-3.

[53] M.T. Ortega, J.E. Riviere, K. Choi, N.A. Monteiro-Riviere, Biocorona formation on gold nanoparticles modulates human proximal tubule kidney cell uptake, cytotoxicity and gene expression, Toxicol. In Vitro 42 (2017) 150–160, https://doi.org/10.1016/j.tiv.2017.04.020.

[54] M. Lundqvist, J. Stigler, T. Cedervall, T. Berggård, M.B. Flanagan, I. Lynch, G. Elia, K. Dawson, The evolution of the protein corona around nanoparticles: a test study, ACS Nano 5 (2011) 7503–7509, https://doi.org/10.1021/nn202458g.

[55] M.S. Ehrenberg, A.E. Friedman, J.N. Finkelstein, G. Oberdörster, J.L. McGrath, The influence of protein adsorption on nanoparticle association with cultured endothelial cells, Biomaterials 30 (2009) 603–610, https://doi.org/10.1016/j.biomaterials.2008.09.050.

[56] L. Vroman, A.L. Adams, G.C. Fischer, P.C. Munoz, Interaction of high molecular weight Kininogen, Factor XII, and Fibrinogen in plasma at interfaces, 55 (1980) 156–159.

[57] S. Shahabi, S. Döscher, T. Bollhorst, L. Treccani, M. Maas, R. Dringen, K. Rezwan, Enhancing cellular uptake and doxorubicin delivery of mesoporous silica nanoparticles via surface functionalization: effects of serum, ACS Appl. Mater. Interfaces 7 (2015) 26880–26891, https://doi.org/10.1021/acsami.5b09483.

[58] M. Piludu, L. Medda, F. Cugia, M. Monduzzi, A. Salis, Silver enhancement for transmission electron microscopy imaging of antibody fragment-gold nanoparticles conjugates immobilized on ordered mesoporous silica, Langmuir 31 (2015) 9458–9463, https://doi.org/10.1021/acs.langmuir.5b02830.

[59] S. Brunauer, P.H. Emmett, E. Teller, Adsorption of gases in multimolecular layers, J. Am. Chem. Soc. 60 (1938) 309–319, https://doi.org/10.1021/ja01269a023.

[60] E.P. Barrett, L.G. Joyner, P.P. Halenda, The determination of pore volume and area distributions in porous substances. I. computations from nitrogen isotherms, J. Am. Chem. Soc. 73 (1951) 373–380, https://doi.org/10.1021/ja01145a126.

[61] J. Coates, In: Interpretation of Infrared Spectra, A Practical Approach, in: Encyclopedia of Analytical Chemistry, John Wiley & Sons, Ltd, Chichester, UK, 2000, pp. 10815–10837, https://doi.org/10.1002/9780470027318.a5606.

[62] T.-P. Liu, S.-H. Wu, Y.-P. Chen, C.-M. Chou, C.-T. Chen, Biosafety evaluations of well-dispersed mesoporous silica nanoparticles: towards in vivo-relevant conditions, Nanoscale 7 (2015) 6471–6480, https://doi.org/10.1039/C4NR07421A.

[63] M. Since, A Study of the Amide III Band by FT-IR Spectrometry of the Secondary Structure of Albumin, Myoglobin, and " y-Globulin, 41 (1987) 180–184.

[64] G. Sekar, S. Sugumar, A. Mukherjee, N. Chandrasekaran, Multiple spectroscopic studies of the structural conformational changes of human serum albumin — Essential oil based nanoemulsions conjugates, J. Lumin. 161 (2015) 187–197, https://doi.org/10.1016/j.jlumin.2014.12.058.

[65] A. Pielesz, D. Binia, E. Sarna, J. Paluch, W. Waksma, Spectrochimica Acta Part A: molecular and biomolecular spectroscopy the role of topically applied L -ascorbic acid in ex-vivo examination of burn-injured human skin, 185 (2017) 279–285. doi:10.1016/j.saa.2017.05.055.

[66] Z. Zhou, X. He, M. Zhou, F. Meng, Chemically induced alterations in the characteristics of fouling-causing bio-macromolecules – Implications for the chemical cleaning of fouled membranes, Water Res. 108 (2017) 115–123, https://doi.org/10.1016/j.watres.2016.10.065.

[67] K. Kaiden, T. Matsui, S. Tanaka, A Study of the Amide III Band by FT-IR Spectrometry of the Secondary Structure of Albumin, Myoglobin, and γ –Globulin, Appl. Spectrosc. 41 (1987) 180–184, https://doi.org/10.1366/000370287774986714.

[68] A. Salis, M. Boström, L. Medda, F. Cugia, B. Barse, D.F. Parsons, B.W. Ninham, M. Monduzzi, Measurements and theoretical interpretation of points of zero charge/potential of BSA protein, Langmuir 27 (2011) 11597–11604, https://doi.org/10.1021/la2024605.

[69] S.H. Brewer, W.R. Glomm, M.C. Johnson, M.K. Knag, S. Franzen, Probing BSA binding to citrate-coated gold nanoparticles and surfaces, Langmuir 21 (2005) 9303–9307, https://doi.org/10.1021/la050588t.

[70] L. Medda, B. Barse, F. Cugia, M. Boström, D.F. Parsons, B.W. Ninham, M. Monduzzi, A. Salis, Hofmeister challenges: ion binding and charge of the BSA protein as explicit examples, Langmuir 28 (2012) 16355–16363, https://doi.org/10.1021/la3035984.

[71] D.F. Parsons, A. Salis, Current opinion in colloid & interface science hofmeister effects at low salt concentration due to surface charge transfer, Curr. Opin. Colloid Interface Sci. 23 (2016) 41–49, https://doi.org/10.1016/j.cocis.2016.05.005.

[72] M. Piras, A. Salis, M. Piludu, D. Steri, M. Monduzzi, 3D vision of human lysozyme adsorbed onto a SBA-15 nanostructured matrix, Chem. Commun. 47 (2011) 7338–7340, https://doi.org/10.1039/c1cc11840d.